DOI: 10.24352/UB.OVGU-2017-002 TECHNISCHE MECHANIK, 36, 3, (2016), 155 – 165
submitted: July 6, 2016

Numerical Study of the Deformation Behavior of Eutectic Cu/Ag Polycrystals

S. Dodla, A. Bertram

Many materials in nature have a complex structure at different length scales, which influence the material behavior. In the current work, we have investigated the deformation behavior of eutectic Cu/Ag composites with a lamellar structure inside the grains. In particular, the deformation process by uniaxial compression, uniaxial tension, and simple shear have been studied. In order to simulate the deformation behavior of the eutectic Cu/Ag composites, an elasto-viscoplastic continuum model has been implemented considering the initial texture (500 grains) from the experimental data. The numerical simulations have been carried out using the finite element software ABAQUS. The deformation behavior and the simulated texture are correlated to experimental results and discussed.

Notation. We use a symbolic notation given in the continuum mechanics text book (Bertram, 2012). Scalars, vectors, second-order and fourth-order tensors are denoted by a, $\mathbf{a}$, $\mathbf{A}$, and A, respectively. The scalar, dyadic, and Rayleigh product are given by $\cdot$, $\otimes$, and $*$, respectively, where $\mathbf{a}\cdot\mathbf{b} := a_i b_i$, $\mathbf{a}\otimes\mathbf{b} := a_i b_j \mathbf{e}_i \otimes \mathbf{e}_j$, $\mathbf{A} * C := C_{ijkl}\mathbf{A}\mathbf{e}_i \otimes \mathbf{A}\mathbf{e}_j \otimes \mathbf{A}\mathbf{e}_k \otimes \mathbf{A}\mathbf{e}_l$. : denotes the double contraction between tensors, *i.e.*, $\mathbf{A} : \mathbf{B} := A_{ij}B_{ij}$. $\mathbf{A}^T$, $\mathbf{A}^{-1}$ and $\dot{\mathbf{A}}$ denote the transpose, the inverse, and the material time derivative of a second-order tensor $\mathbf{A}$. The linear mapping of a second-order tensor $\mathbf{A}$ by a fourth-order tensor C is written as $C\,[\mathbf{A}]$.

1 Introduction

Cu-Ag polycrystals are widely used in magnet research and applications because of their high strength and high conductivity (Asano et al., 1993; Sakai and Schneider-Muntau, 1997). The eutectic structure of Cu-Ag produces high strength compared to other Cu-Ag compositions. The eutectic Cu-Ag polycrystal shows a two phase lamellar structure inside the grains strengthened with Cu and Ag laminates. Both Cu and Ag lamella phases inside the microstructure present a lamellar ordered face centered cubic (fcc) lattice structure. The lamellar Cu-Ag polycrystal shows an ultimate tensile strength above 700 MPa with increase in the drawing strain (Grünberger et al., 2001; Heringhaus, 1998), and a difference in strain hardening in tension and compression (Shen et al., 2007). The strength and hardening effects are influenced by the grain size, lamellar nanostructure and corresponding volume fraction of each phase. In order to study micro-structural effects on the mechanical properties, a physics based model is required to capture the lamellar information at the micro scale, grain information at meso scale, and the effective behavior at the macro scale to design the structural components.

In the past 20 years multiscale modeling is the common finite element (FE) approach to study the deformation process and the texture evolution of the multi-phase materials. With this method, an elasto-viscoplastic phenomenological model has been applied to study the deformation behavior of eutectic Cu/Ag composites at three different scales (micro, meso, and macro). The micro scale represents the two phase lamellar structure of Cu/Ag phases, the meso scale represents the grain structure, and the macro scale represents the homogenized deformation behavior of the material. Artificial homogenization from micro to meso scale has been done using projection criteria i.e., amplifying the lamella scale to fit into grain scale. The amplification has been done since the lamellae (micro scale) and the grains (meso scale) live on rather different length scales. And the numerical homogenization between the meso and macro scale has been done by means of the finite element method. The micro scale captures the lamellar structure present inside the grain, the meso scale allows to capture the grain structure present inside the material, and the macro scale for computing the homogenized deformation behavior. The majority of early works have used the micro structure information of a single phase, because finite element calculations of the microstructure for the multiphase materials are computationally expensive. Our previous work (Dodla et al., 2015a) is focused on the RVE with 100 grains along with a Cu/Ag lamellar structure to study the compressive flow behavior. In the current work, the FE based multiscale modeling approach is used to study the deformation process (uniaxial compression,

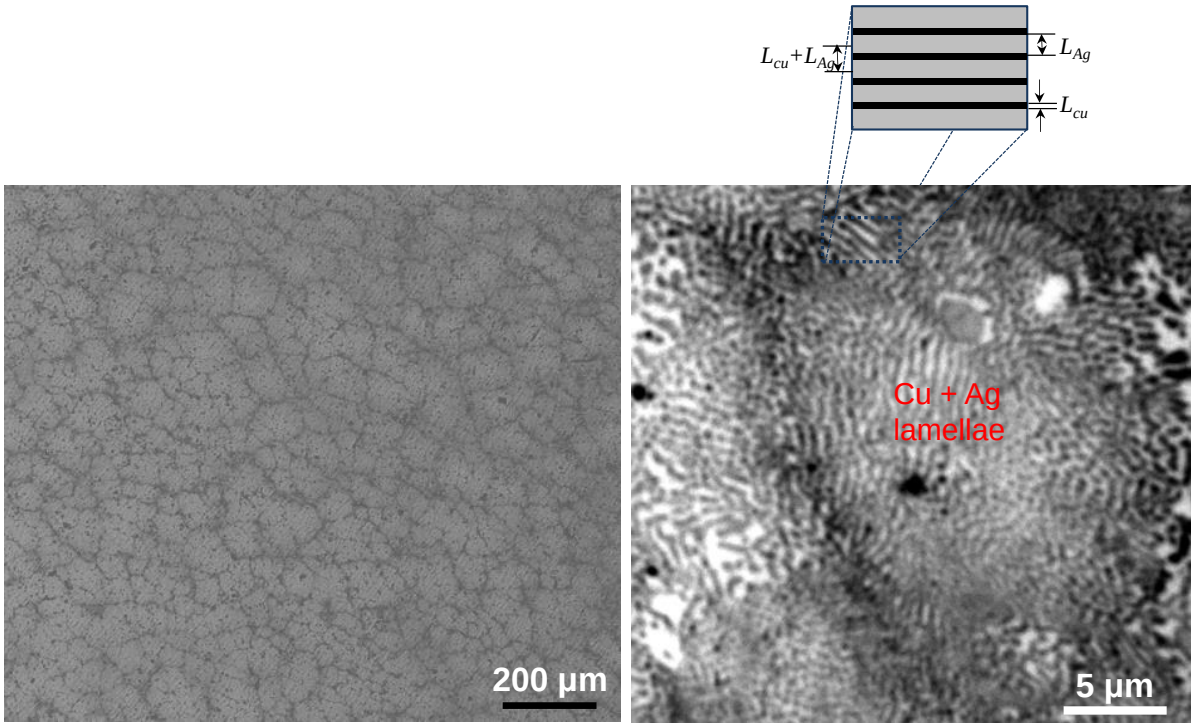

Figure 1: Optical microscopy images in transverse section of Cu-Ag ingot showing the different information at the grain scale (left) and at the lamellae scale along with lamella spacing (right)

uniaxial tension, and simple shear) of lamellar Cu/Ag phases with 500 grains.

2 Initial Texture

After secondary processing (cold rolling, cold drawing) for many materials the strength will increase. The enhance in mechanical strength is believed to be instantly related to the refinement of the microstructure (Misra et al., 2004) and the lattice distortion in the materials (Han and Yu-Zhang, 2004). In the current work we consider a cold drawn rod having a diameter of 12.42 mm (more details about the manufacturing process, micro structure, and initial texture are given in (Dodla et al., 2015b)). Fig. 1 presents the microstructure of the cold drawn sample. Fig. 1 are the optical microscopy images taken from sample in the cold drawn condition showing the combination of grains with an average grain size of 50 μm, lamellar Cu/Ag eutectic regions. The selected region in Fig. 1 (right) shows the average lamella spacing ($L_{Cu} + L_{Ag}$) and the periodic layers of Cu (L_{Cu}) and Ag (L_{Ag}) lamella. X-ray analysis is used to determine the texture of a cold drawn rod. XRD measurements are performed by using an X-ray tube with Chromium-anode in point focus mode and 1D detector with secondary K_β filtering. The texture measurements were done at central location of the cold drawn rod in longitudinal direction. From the experimental investigations (Dodla, 2015), it is observed that the misorientation angle in the lamellar region inside the grain lies below 10^o. Hence in the numerical simulations we assume that each lamella (Cu, Ag) inside the grain has the same initial crystallographic orientation with respect to the grain. The measured texture of the Cu phase has been approximated by 500 grains as a compromise between precision and computational costs. The texture is represented in terms of a pole figure and the ODF. Figure 1 (top) represents the measured texture of the sample material in terms of a (100) pole figure and $\phi_2(= 45^o)$ sections of the orientation distribution function (ODF) in the space of Euler angles ($\phi_1 \leq 90^o$, $\Phi \leq 90^o$). Figure 1 (bottom) represents the texture approximated by 500 grains. The Euler angles ϕ_1, Φ, ϕ_2 are given in 'ZXZ' convention (Bunge, 1993).

3 Material Model

An elasto-viscoplastic single crystal constitutive model is implemented for the lamellar structure of the Cu and Ag phases. The model is based on the concept of isomorphic elastic ranges (Bertram, 2012). The evolution of the plastic deformation is accounted for by means of a second-order tensor, called plastic transformation **P**. The tensor **P** relates the variables in the undistorted placement to the reference placement. In the following equations, tilde

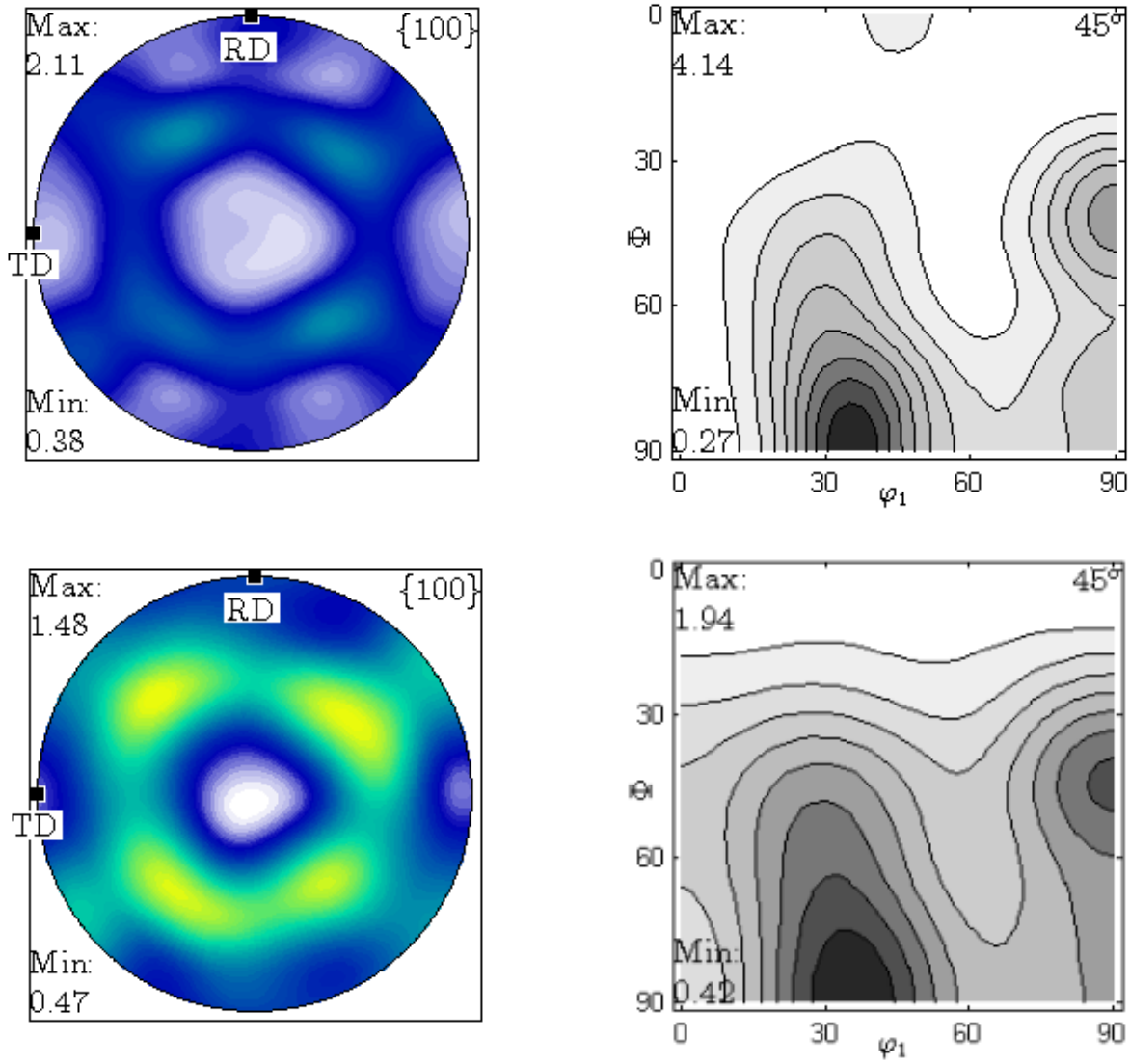

Figure 2: Measured (top) and approximated (bottom) (100) pole figure and ϕ_2 section of 45^o of ODF by 500 discrete orientations

$(\sim)$ refers to all variables which are described with respect to the initially undistorted lattice base.

3.1 Constitutive Law

This approach is based on the assumption of isomorphic elastic laws in all elastic ranges of our elasto-plastic material point. If we express the elastic law in the current elastic range by a function k_p that relates the right Cauchy-Green tensor $\mathbf{C} := \mathbf{F}^T\mathbf{F}$ to the second Piola-Kirchhoff stress tensor $\mathbf{T}^{2PK} := det(\mathbf{F})\mathbf{F}^{-1}\mathbf{T}\mathbf{F}^{-T}$ as

$$\mathbf{T}^{2PK} = k_p(\mathbf{C}) \tag{1}$$

then the isomorphy condition can be used to transform this elastic law into a (constant) elastic reference law k_0 as

$$k_p(\mathbf{C}) = \mathbf{P}k_0(\mathbf{P}^T\mathbf{C}\mathbf{P})\mathbf{P}^T \tag{2}$$

by a unimodular plastic transformation $\mathbf{P}$ (see Bertram (2012)). If we concentrate on a linear St. Venant-Kirchhoff law for k_p

$$\mathbf{T}^{2PK} = \frac{1}{2}\tilde{K}[\mathbf{C} - \mathbf{C}_u] = \tilde{K}[\tilde{\mathbf{E}}^G] \tag{3}$$

with the Green strain tensor $\tilde{\mathbf{E}}^G = \frac{1}{2}(\mathbf{C} - \mathbf{C}_u)$ with respect to some unloaded configuration $\mathbf{C}_u$, then the above isomorphy condition leads to an elastic reference law

$$\mathbf{T}^{2PK} = \frac{1}{2}K[\mathbf{C} - \mathbf{I}] = K[\mathbf{E}^G] \tag{4}$$

with $\tilde{K} = \mathbf{P} * K$, $\mathbf{C}_u = \mathbf{P}^{-T}\mathbf{P}^{-1}$ and $\mathbf{E}^G = \frac{1}{2}(\mathbf{C} - \mathbf{I})$. $\tilde{K}$ denotes the fourth-order constant stiffness tetrad for a cubic crystal. The stiffness tetrad is represented by a six by six Voigt matrix, and the components refer to the normalised orthonormal basis $\mathbf{B}_\alpha$ of symmetric second-order tensors (Böhlke and Bertram, 2001; Cowin, 1989; Böhlke, 2001), i.e., $K_{\alpha\beta} = \mathbf{B}_\alpha : K\,[\mathbf{B}_\beta]$
Copper and silver materials have a face centered cubic (fcc) crystal structure. The three independent elastic constants for copper and silver are taken from (Kalidindi and Anand, 1993), (Dodla et al., 2015a).

3.2 Flow Rule

In general, fcc materials exhibit crystallographic slip in $\{111\}\langle 110\rangle$ slip systems. These 12 primary slip systems are described by the Schmid tensors $\tilde{\mathbf{S}}^\alpha := \tilde{\mathbf{d}}_\alpha \otimes \tilde{\mathbf{n}}^\alpha$, which are given by the slip direction $\tilde{\mathbf{d}}_\alpha$ and the slip plane normal $\tilde{\mathbf{n}}^\alpha$. The resolved shear stress τ^α in a slip system α can be calculated as

$$\tau^\alpha := \tilde{\mathbf{C}}\tilde{\mathbf{T}}^{2PK} : \tilde{\mathbf{S}}^\alpha \tag{5}$$

An evolution of the plastic transformation $\mathbf{P}$ is given in terms of the shear rate $\dot{\gamma}_\alpha$ and the Schmid tensors $\tilde{\mathbf{S}}^\alpha$

$$\mathbf{P}^{-1}\dot{\mathbf{P}} = -\sum_\alpha \dot{\gamma}^\alpha \tilde{\mathbf{S}}^\alpha \tag{6}$$

The kinetics of dislocation motion have been elaborated by the relationships between the resolved shear stress and the plastic shear rate $\dot{\gamma}^\alpha$ of the slip system α by using the power law (Hutchinson, 1976)

$$\dot{\gamma}^\alpha = \dot{\gamma}_0 \mathrm{sgn}(\tau^\alpha)\ |\frac{\tau^\alpha}{\tau_c(\gamma)}|^m \tag{7}$$

where $\dot{\gamma}_0$ is a constant reference shear rate, and the exponent m determines the strain sensitivity of the material. The initial conditions of the evolution equation (6) are $\tilde{\mathbf{F}}\,(t=0) = \mathbf{Q}\,(t=0) \in SO(3)$. The orientation of the crystal is given by a proper orthogonal tensor $\mathbf{Q}\,(t) := \mathbf{g}_i\,(t) \otimes \mathbf{e}_i$. Here $\{\mathbf{e}_i\}$ is the orthonormal vector base of a fixed Cartesian coordinate system, and $\{\mathbf{g}_i\}$ is the orthonormal lattice vector base. The initial resolved shear stress at time $t = 0$ is given as $\tau_c\,(0) = \tau_{c_0}$.

3.3 Hardening Rule

A simple, most popular ansatz for the two types of hardening (self and latent) is the linear hardening rule (Hill, 1966), (Bertram, 2012).

$$\dot{\tau_c}^\alpha = \sum_\beta h_{\alpha\beta}\dot{\gamma}^\beta, \quad h_{\alpha\beta} = q_{\alpha\beta}\theta\,(\gamma) \tag{8}$$

where $\theta(\gamma) = \frac{\mathrm{d}\tau_c^\alpha}{\mathrm{d}\gamma}$ and $q_{\alpha\beta}$ are the matrix components which account for self and latent hardening of the crystal. For the fcc cubic crystal having 12 $\{111\}\langle 110\rangle$ primary slip systems, we consider $q_{\alpha\beta}$ equal to 1.0 for the coplanar slip systems and equal to 0.9 for noncoplanar systems (Beyerlein et al., 2011). The evolution of the critical resolved shear stress of all slip systems as a function of shear γ is described by a Voce-type hardening law (Voce, 1955)

$$\tau_c^\alpha = \tau_{c_0} + (\tau_s + \theta_\infty\gamma)(1 - \exp(-\theta_0\gamma/\tau_s)) \tag{9}$$

with

$$\gamma = \int \sum_\alpha |\dot{\gamma}_\alpha|\ \mathrm{dt} \tag{10}$$

γ is given as an integral over the sum of shear rates of all slip systems. The Voce type hardening rule contains four hardening parameters, namely the initial resolved shear stress τ_{c_0}, a saturation stress τ_s, an initial hardening modulus θ_0, and a remaining hardening modulus θ_∞. The material model has been implemented into the user subroutine (UMAT) of the finite element package (ABAQUS) (ABAQUS, 1990). A Newton-Raphson iteration has been performed using a backward Euler scheme (Böhlke et al., 2006).

4 Deformation Process

To study the mechanical behavior and the respective texture development, numerical experiments have been performed like uniaxial tension, uniaxial compression, and simple shear. The deformation process is prescribed in terms of the macroscopic deformation gradient **F** or the velocity gradient $\mathbf{L} = \dot{\mathbf{F}}\mathbf{F}^{-1}$. For prescribing the deformation gradient, the motion is assumed to be isochoric, i.e., $det\mathbf{F} = 1$. The deformation gradient is expressed by the velocity gradient **L** as

$$\mathbf{F}(t) = \exp(\mathbf{L}t)\mathbf{F}_0 \tag{11}$$

Initially, $\mathbf{F}_0$ is given as the second-order identity tensor **I**.

5 Representative Volume Element (RVE)

Three-dimensional FE simulations are performed by the finite element software (ABAQUS, 1990). Our RVE with periodic boundary conditions has a Poisson-Voronoi micro structure (Kumar and Kurtz, 1994). In the present work, the experimental data for uniaxial compression of eutectic Cu/Ag composite was compared with numerical finite element simulations. Besides the numerical predictions (uniaxial tension, simple shear) with the flow behavior and the crystallographic texture are numerically investigated in eutectic Cu/Ag composite. From the experimental data (Dodla et al., 2015b), the average grain size is 50 μm and the average lamella spacing $(L_{Cu} + L_{Ag})$ is 265 nm. For each grain we need approximately 190 lamellae spacing $(L_{Cu} + L_{Ag})$. Moreover for each lamella a minimum of 2 elements is required to study the lamellar behavior. In total 380 elements are required for each grain. Due to the computational limitations, each side of the RVE is modeled by only 40 elements. The element size on each side of the RVE is fixed based on the minimum thickness of lamella and the number of elements on each side. We fixed the element size by 0.05 in all our numerical simulations with 500 grains. The predicted material parameters shown in Table 1.

The finite element model for the simulation of the lamellar structure with 500 grains is shown in Fig. 3. Fig. 3A (left) represents 500 grains. Each grain corresponds to a different orientation. The grains are visualised in the figure. Fig. 3A (right) presents the lamellar structure of Cu and Ag. In these simulations, the microstructure (grains, Cu/Ag lamellae) is given as regular Voronoi tessellations, and the boundary conditions are periodic. The RVE mesh convergence study is first conducted to study mesh sensitivity of the results. The deformation behavior has to be investigated until convergence is achieved. The RVE mesh consists of 64,000 linearly fully integrated hexahedral elements. More information about the simulation procedure has been given in (Dodla et al., 2015a). The RVE is subjected to uniaxial compression, uniaxial tension, and simple shear as shown in Fig. 3B, 3C, and 3D.

6 Simulated Results

The simulated results are presented in terms of stress-strain responses and the crystallographic texture. The measured and simulated stress-strain curves under compression are shown in Fig. 4. In this figure, the stress-strain behavior from the experiments is shown using dotted lines, while the stress-strain response from the RVE approach is shown using solid lines. The elasto-viscoplastic material model is applied in the numerical simulations

Table 1: Flow rule and hardening parameters

Material	$\dot{\gamma}_0$ [s^{-1}]	m [-]	$\tau_{c_0}[MPa]$	$\tau_s[MPa]$	$\theta_0[MPa]$	$\theta_\infty[MPa]$
Cu	0.0001	80	5.5	167.6	7964	9.2
Ag	0.0001	80	5	200.9	4501	20

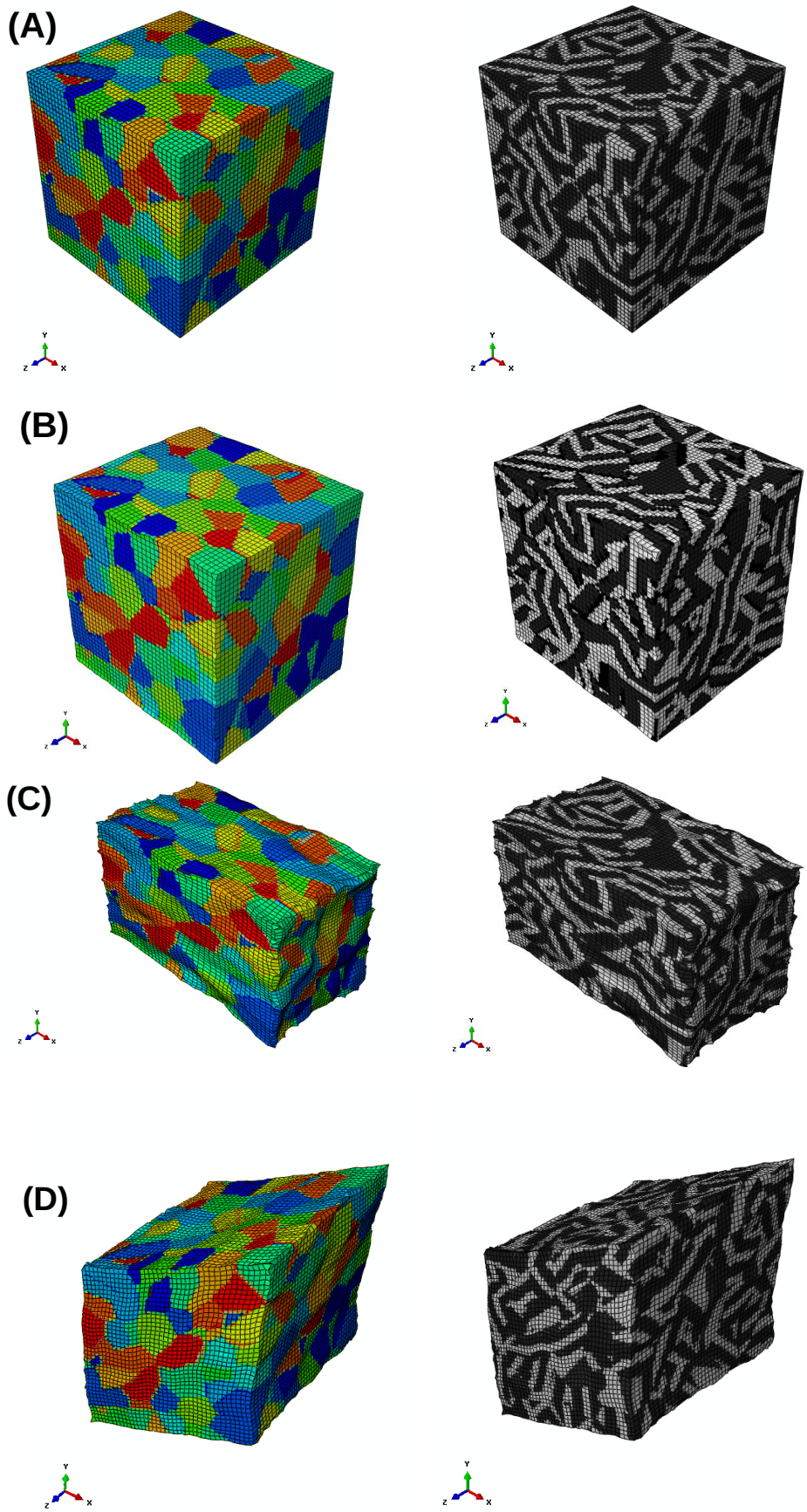

Figure 3: (A) RVE with 64,000 elements containing 500 grains (left) and Cu/Ag lamellar structure inside the grains, (B) RVE with compressive deformation along Z direction, (C) RVE with tensile deformation in X direction, (C) RVE with shear deformation in XY plane.

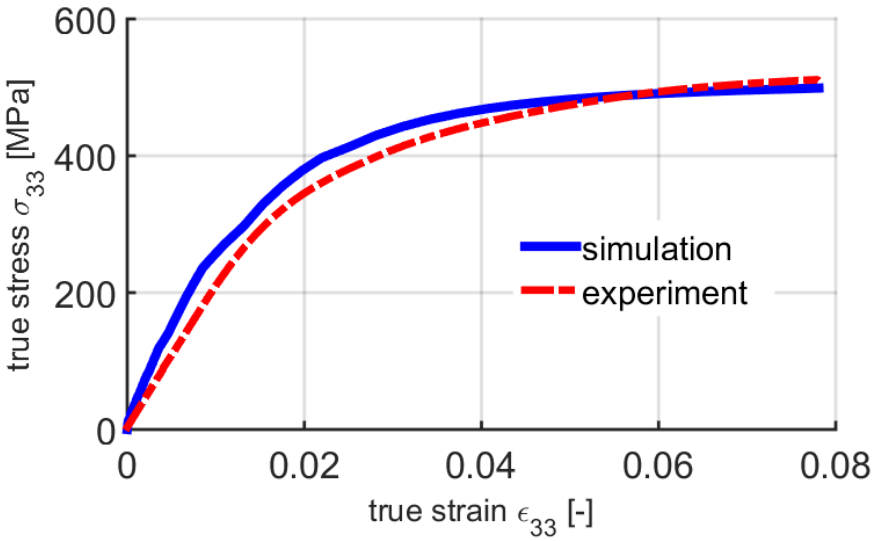

Figure 4: Numerical simulation and experimental true stress-strain data of Cu-Ag eutectic composite in simple compression

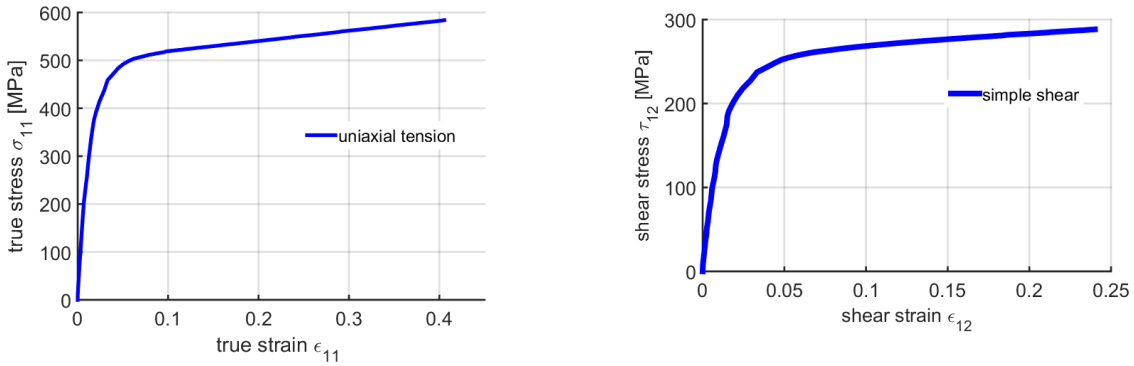

Figure 5: Stress-strain curves of the simple tension (bottom left), and the simple shear (bottom right)

to validate the deformation behavior. The simulated RVE successfully validates the flow behavior in the deformation zone (hardening). In the case of an initial slope, there is a slightly mismatch with the experimental data. There are different possibilities for the deviation in the initial slope with the experimental data such as heterogeneity in the microstructure, internal stresses and the elastic constants of Cu/Ag single crystals. Previous studies (Han et al., 1999; Baldwin, 1949; Denton, 1966) have reported considerable internal stresses in drawn composites due to the compatibility required during co-deformation. Hence these internal stresses may lead to the rounding of the flow curves in the elastic region.

The tensile test is the alternate method for the investigation of material properties. Fig. 5 (left) shows the true stress-strain curves simulated under uniaxial tension. As seen in Fig. 4 and Fig. 5 (left), the stress-strain behavior under uniaxial compression and uniaxial tension is identical in the elastic region. However, the strain hardening in tension is slightly higher than under compression. It is often observed that the stress-strain curves under tension and compression coincide to a certain degree when they are plotted in terms of true stress against true strain (Lubliner, 2006). A numerical test of simple shear is used to determine the shear stress vs shear strain response and the crystallographic texture evolution. Simulated results for the shear stress τ_{12} vs the shear strain ϵ_{12} in xy plane on the eutectic Cu/Ag composite are shown in Fig. 5 (right). From the numerical stress-strain plot (Fig. 5 (right)), a smooth transition from the elastic to the plastic behavior is observed. This numerical approach can be applied for the comparison of experimental shear tests.

The crystallographic texture is presented in terms of the $\phi_2 (= 0^o - 90^o)$ sections in steps of 5^o of the orientation

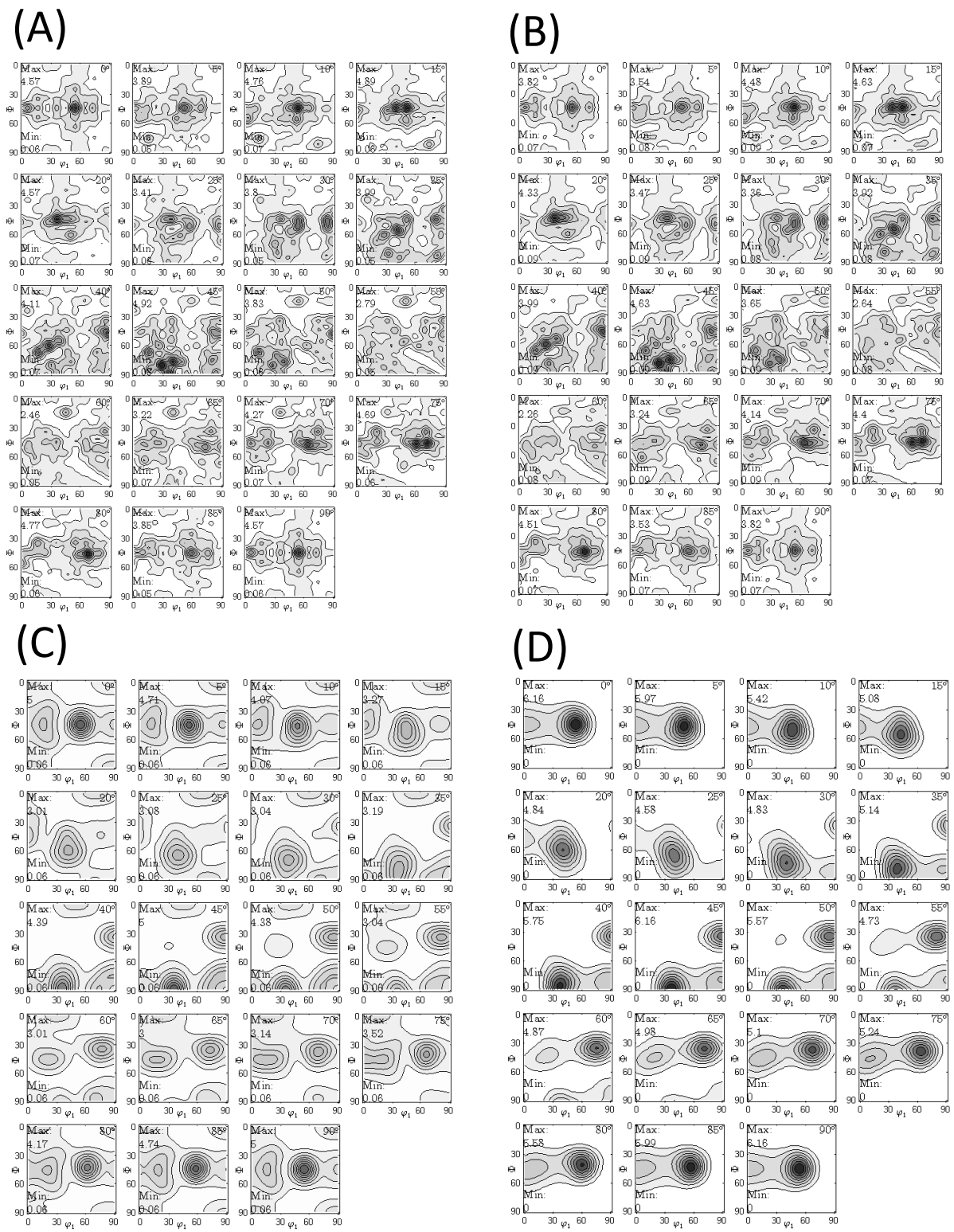

Figure 6: Simulated (A, B) and measured (Dodla, 2015) (C, D) ODF for selected sections in the orientation space in the case of uniaxial compression (A and C) Cu phase, and (B and D) Ag phase.

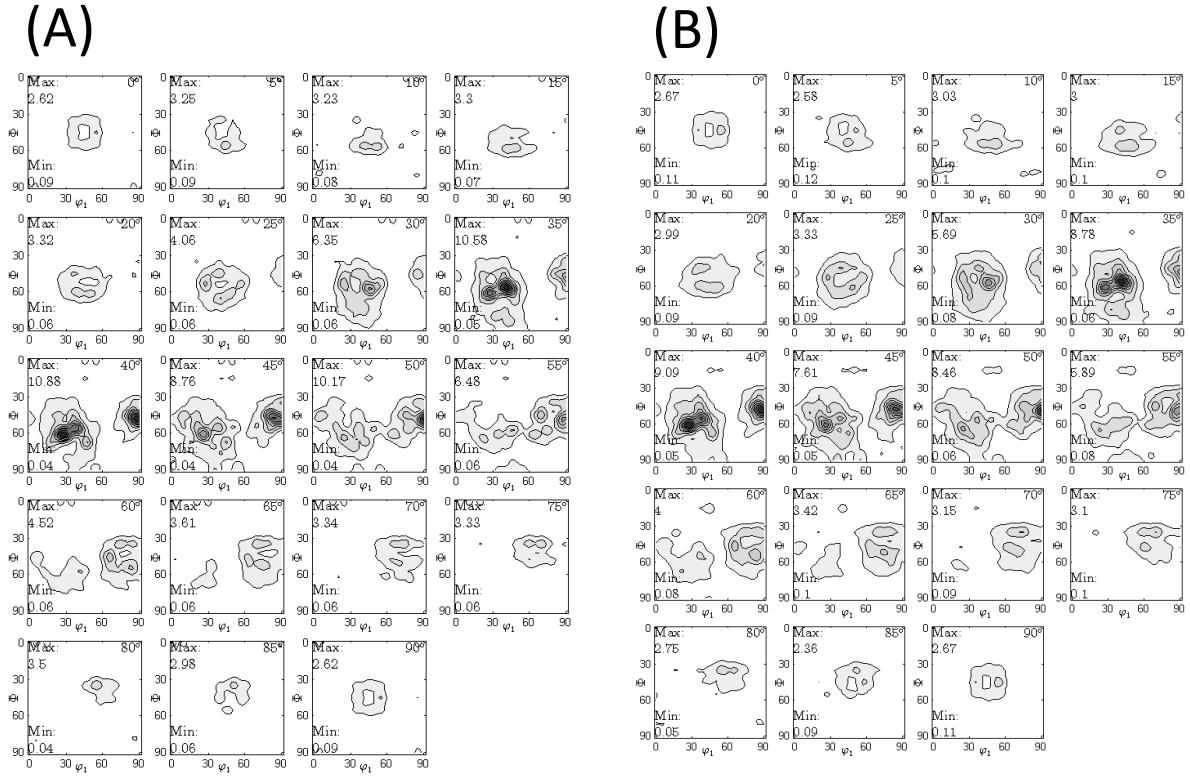

Figure 7: Simulated ODF for selected sections in the orientation space in the case of uniaxial tension (A) Cu phase, and (B) Ag phase.

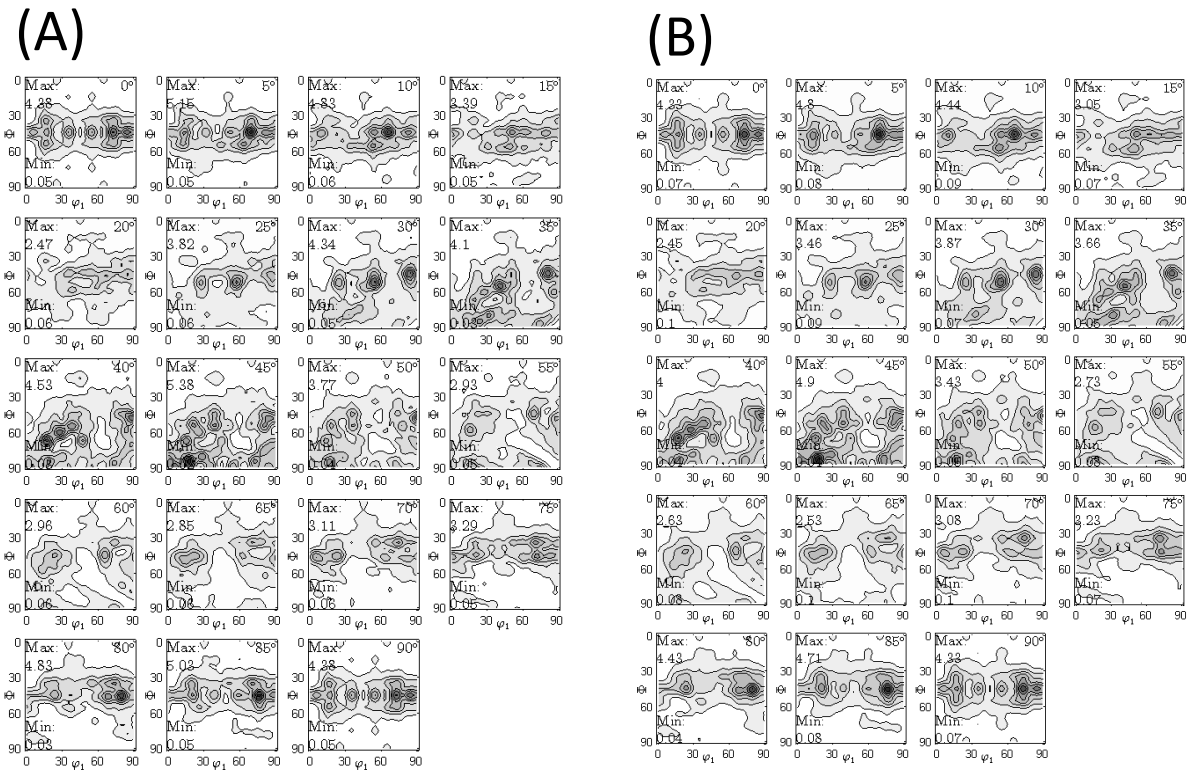

Figure 8: Simulated ODF for selected sections in the orientation space in the case of simple shear (A) Cu phase, and (B) Ag phase.

distribution function (ODF) in the space of Euler angles ($\phi_1 \leq 90^o, \Phi \leq 90^o$). The simulated texture in terms of the ODF is compared with the experimental measured texture for both Cu and Ag phases in simple compression in Fig. 6. The numerical simulations reproduce the experimentally observed textures for the Cu and Ag phases. The simulated texture of Cu and Ag phases in Fig. 6 are identical due to the initial approximation of same texture for both phases. The measured and simulated ODF consists of important texture components (Copper orientation ($90^o, 35^o, 45^o$), Brass orientation ($35^o, 45^o, 0^o$), Goss orientation ($0^o, 45^o, 0^o$)). The agreement between the measured and simulated ODF is good (see Fig. 6). It is clear from experiments (Beyerlein et al., 2011; Dodla et al., 2015b) that the dominant texture in Cu-Ag eutectic composites is a Brass-type texture. From the numerical simulations of different deformation processes, the dominant texture component is Brass (see Fig. 6 - 8). However there is a shift in the locations of the peak intensities in the orientation space. Note that the texture intensity in the Cu phase is slightly higher than the Ag phase for all deformation processes. This is because the harder phase (Cu) has a stronger influence on texture evolution compared to the softer phase (Ag).

7 Summary

A multiscale modeling approach is introduced to study the deformation process of nanostructured lamellar Cu-Ag polycrystals. It has been shown that the finite element simulation (RVE) captures the Cu/Ag lamellar structure inside the 500 grains. The deformation behavior of each lamella (Cu/Ag) phase is given by the elasto-viscoplastic single crystal constitutive model. In addition, the developed multiscale FE model is able to capture the texture of each phase. In the case of simple compression there is a good agreement between the measured and simulated ODF for both phases. It is shown that the dominant texture of lamellar Cu-Ag polycrystals are Brass-type texture for all deformation process. In the current work the dislocation slip is used as a deformation mechanism that accounts for plastic deformation at room temperature. Nevertheless there is room for improvement of the material model on the meso scale (grain) by including, e.g., deformation induced by twinning. To understand the effect of twinning on the deformation behavior, studies of various deformation tests (tensile, compression, shear) considering slip and twinning as a deformation mechanism for plastic deformation need to be incorporated.

8 Acknowledgements

The financial support provided by the German Science Foundation (DFG) through GRK 1554 is gratefully acknowledged.

References

ABAQUS: *Reference Manuals, Hibbitt, Karlsson and Sorensen*. Addison-Wesley, Inc., Providence, RI (1990).

Asano, T.; Sakai, Y.; Inoue, K.; Oshikiri, M.; Maeda, H.: High-field pulsed magnet wound of Cu-Ag alloy wire. *Japanese Journal of Applied Physics*, 32, (1993), L1027–L1029.

Baldwin, W. M.: Residual stresses in metals. *Proceeding, American Society for Testing Materials*, 49, (1949), 539–583.

Bertram, A.: *Elasticity and Plasticity of Large Deformations - an Introduction, Third Edition*. Springer Verlag, Berlin (2012).

Beyerlein, I. J.; Mara, N. A.; Bhattacharyya, D.; Alexander, D. J.; Necker, C. T.: Texture evolution via combined slip and deformation twinning in rolled silver-copper cast eutectic nanocomposite. *International Journal of Plasticity*, 27, (2011), 121–146.

Böhlke, T.: *Crystallographic Texture Evolution and Elastic Anisotropy: Simulation, Modeling and Applications*. Shaker Verlag, Aachen (2001).

Böhlke, T.; Bertram, A.: The evolution of Hooke's law due to texture development in FCC polycrystals. *International Journal of Solids and Structures*, 38, (2001), 9437–9459.

Böhlke, T.; Risy, G.; Bertram, A.: Finite element simulation of metal forming operations with texture based material models. *Modelling and Simulation in Material Science and Engineering*, 14, (2006), 365–387.

Bunge, H.: *Texture Analysis in Materials Science*. Curvillier Verlag, Göttingen (1993).

Cowin, S.: Properties of the anisotropic elasticity tensor. *Quarterly J. of Mechanics & Appl. Maths*, 42, (1989), 249–266.

Denton, A. A.: Determination of residual stress. *Metall. Rev.*, 11, (1966), 1–23.

Dodla, S.: *Experimental Investigations and Numerical Simulations of Lamellar Cu-Ag Composites*. Barleben: Docupoint Verlag. Dissertation, Fakultät für Maschinenbau, Otto-von-Guericke-Universität Magdeburg (2015).

Dodla, S.; Bertram, A.; Krüger, M.: Finite element simulation of lamellar copper-silver composites. *Computational Materials Science*, 101, (2015a), 29–38.

Dodla, S.; Thiem, P.; Krüger, M.; Dietrich, D.; Bertram, A.: Microstructure, flow behavior, and bulk texture evolution of cold drawn copper-silver composites. *Journal of Alloys and Compounds*, 647, (2015b), 519–527.

Grünberger, W.; Heilmaier, M.; Schultz, L.: Development of high-strength and high-conductivity conductor materials for pulsed high-field magnets at Dresden. *Physica B*, 45, (2001), 643–647.

Han, K.; Embury, J. D.; Sims, J. R.; Campbell, L. J.; Schneider Muntau, H. J.; Pantsyrnyi, V. I.; Shikov, A.; Nikulin, A.; Vorobieva, A.: The fabrication, properties and microstructure of Cu-Ag and Cu-Nb composite conductors. *Materials Science and Engineering A*, 267, (1999), 99–114.

Han, K.; Yu-Zhang, K.: Transmission electron microscopy study of metallic multilayers. *Scripta Materialia*, 50, (2004), 781–786.

Heringhaus, F.: *Quantitative Analysis of the Influence of th Microstructure on Strength, Resistivity, and Magnetoresistance of Eutectic Silver-Copper*. Shaker Verlag, Berlin (1998).

Hill, R.: Generalized constitutive relations for incremental deformation of metal crystals by multislip. *Journal of the Mechanics and Physics of Solids*, 14, (1966), 95–102.

Hutchinson, J.: Bounds and self-consistent estimates for creep of polycrystalline materials. *Proc. R. Soc. London*, A 348, (1976), 101–127.

Kalidindi, S. R.; Anand, L.: Large deformation simple compression of a copper single crystal. *Metallurgical Transactions A*, 24A, (1993), 989–992.

Kumar, S.; Kurtz, S. K.: Simulation of material microstructure using a 3D Voronoi tesselation: Calculation of effective thermal expansion coefficient of polycrystalline materials. *Acta Metallurgica et Materialia*, 42, (1994), 3917–3927.

Lubliner, J.: *Plasticity Theory*. Macmillan Publishing Company, New York (2006).

Misra, A.; Hirth, J.; Hoagland, R.; Embury, J.; Kung, H.: Dislocation mechanisms and symmetric slip in rolled nano-scale metallic multilayers. *Acta Materialia*, 52, (2004), 2387–2394.

Sakai, Y.; Schneider-Muntau, H. J.: Ultra-high strength, high conductivity Cu-Ag alloy wires. *Acta materials*, 45, (1997), 1017–1023.

Shen, T. D.; Zhang, X.; Han, K.; Davy, C. A.; Aujla, D.; Kalu, P. N.; Schwarz, R. B.: Structure and properties of bulk nanostructured alloys synthesized by flux-melting. *Journal of Materials Science*, 42, (2007), 1638–1648.

Voce, E.: A practial strain-hardening function. *Metallurgia*, 51, (1955), 219–226.

Address:

Srihari Dodla, Wolfson School of Mechanical, Electrical and Manufacturing Engineering, Loughborough University, LE11 3TU, Loughborough, UK, email: 529srihari@gmail.com
A. Bertram, Otto-von-Guericke-Universität Magdeburg, D-39106, Magdeburg, Germany, Tel. +49 391 67 52246; Fax +49 391 67 2863, email: albrecht.bertram@ovgu.de